BL4U

Carbon K-Edge NEXAFS and Sulfur L-Edge NEXAFS Measurements of Samples from Asteroid Ryugu

T. Matsumoto[1]

[1]*The Hakubi Center for Advanced Research, Kyoto University Kitashirakawa-Oiwakecho, Sakyo, Kyoto 606-8502, Japan*

The *Hayabusa2* spacecraft from the Japan Aerospace Exploration Agency (JAXA) explored the asteroid Ryugu and returned surface grains to Earth. It was anticipated that the grains brought back directly from the asteroid might contain previously undiscovered substances not found in meteorites. Among these could be highly water-soluble materials, which readily react with moisture in Earth's atmosphere and are therefore difficult to detect unless examined in their pristine state as preserved in space.

In this study, Ryugu grains were analyzed using FE-SEM and (scanning) transmission electron microscopy ((S)TEM), and synchrotron radiation-based Scanning transmission X-ray microscopy (STXM). Thin sections for STXM and TEM analysis were prepared using a focused ion beam system (FIB). Near edge X- ray absorption fine structure (NEXAFS) spectra at carbon K-edge and sulfur L-edge of FIB sections of Ryugu grain C0071 were measured using the STXM beamline, BL4U. The custom-built sample transfer vessel and a nitrogen-filled glove box were used to prevent sample exposure to the air. The date analysis was performed using the aXis 2000 software.

Using a transmission electron microscope (TEM), which allows observation of structures at the nanometer scale, I identified sodium carbonates (Na_2CO_3 and a hydrate phase), halite crystals (NaCl: sodium chloride) in Ryugu grains. These mineral phases have not been reported in Ryugu samples. The STXM analyses were performed to identify chemical features of these sodium carbonates.

The C K-edge NEXAFS spectrum from the sodium carbonates exhibits a sharp peak at 290.2 eV, which is assigned to the 1s → π transition of carbonate (Fig. 1). Sulfur L-edge in the sodium carbonates of the grain C0071 corresponds to sodium sulfate (Fig. 1). STEM-energy dispersive X-ray spectrometer (EDX) analysis showed that the major elements within the sodium carbonates are sodium (Na), carbon (C), oxygen (O), with minor amounts of sulfur (S) (<6 atomic %) and fluorine (F) (<4 atomic %). STXM analysis suggests that sulfur component detected by STEM-EDS analysis is derived from sodium sulfate included in the sodium carbonate minerals.

The sodium salt minerals are all highly water-soluble. The fact that they dissolve easily in water suggests that their crystallization could only occur if the liquid was extremely limited and had a very high salt concentration. The salt minerals were hypothesized to be formed during the disappearance of the liquid water after the major aqueous minerals found in the Ryugu samples precipitated in the parent body. One possible explanation for the loss of liquid is the evaporation of saltwater. If large-scale fractures formed and connected the interior of the parent body to the outer vacuum environment, the liquid body could have undergone depressurization and evaporation. On Earth, when lakes dry up, highly concentrated saltwater forms, leading to the precipitation of minerals such as sodium carbonate and halite. The remnants of the vaporization are referred to as "evaporites". Similar processes may have occurred in Ryugu's parent body. Another possibility is the freezing of liquid water. After the Ryugu's parent body reached its peak temperature, it cooled due to the exhaustion of the radioactive heat. The remaining alkaline brines probably concentrated as H_2O ices formed. As a result, the sodium salts would have formed at subzero Celsius temperatures. The frozen ice could have sublimated into space over time. Currently, Ryugu shows no signs of large amounts of liquid, nor do its surface grains appear wet. Until now, it was unclear how the liquid water in the parent body was lost. This study has revealed that the loss of liquid water in Ryugu's parent body occurred through evaporation or freezing.

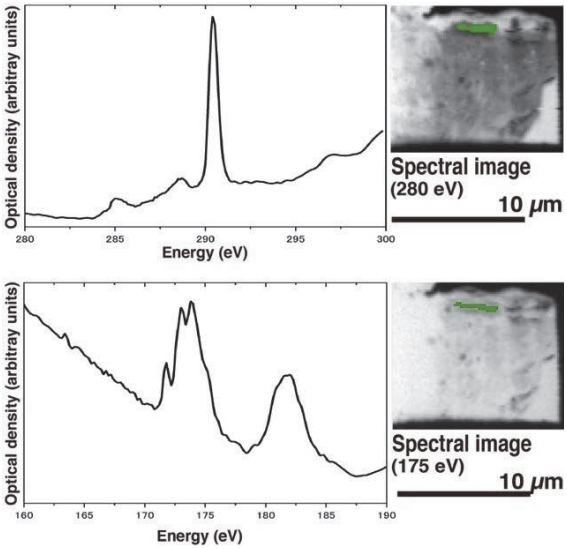

Fig. 1. The C K-edge NEXAFS spectrum (upper figure) and S L-edge NEXAFS spectrum of Ryugu sample(C0071).

[1] T. Mastsumoto *et al.*, *Nature Astronomy*, 8:12, 1536-1543. (2024)

BL4U

Correlation Between Electronic Structures and Supercapacitive Performance of NiCo/Pencil Lead Studied by X-ray Spectro-Microscopy

C. J. Yang[1,2], T. C. Huang[3], H. W. Chang[3], T. Araki[4], T. Ohigashi[4,5], D. H. Wei[2] and C. L. Dong[1]

[1]*Department of Physics, Tamkang University, Tamsui 25137, Taiwan*
[2]*Graduate Institute of Manufacturing Technology, National Taipei University of Technology, Taipei 10608, Taiwan*
[3]*Department of Chemical Engineering, National United University, Miaoli 360302, Taiwan*
[4]*UVSOR Synchrotron Facility, Institute for Molecular Science, Okazaki 444-8585, Japan*
[5]*Photon Factory, High Energy Accelerator Research Organization, Tukuba 305-0801, Japan*

As the issue of energy shortage becomes increasingly serious, electrochemical energy storage is emerging as a highly active research area. Compared with other energy storage devices, supercapacitors have higher charge and discharge cycle life and better stability, while also enabling rapid charging and discharging reactions. The electrodes made of nanostructured nickel-cobalt oxides are not only facile to synthesize, but also offer the advantages such as low cost, high specific capacitances, low resistance, and environmental friendliness [1]. Carbon materials are also widely used as electrode materials due to their porous structure and high specific surface area, which could facilitate the electrothermal reactions and help improve overall performance [2]. In this study, NiCo-oxide nanostructures were prepared on pencil lead. The pencil lead was first activated using HNO_3 to form the activated pencil graphite electrode (APGE), and then treated hydrothermally with varying ratios of $Ni(NO_3)_2 \cdot 6H_2O$ and $Co(NO_3)_2 \cdot 6H_2O$ underwent hydrothermal treatment to obtain the nickel-cobalt oxides with different electrochemical activities.

The Scanning Transmission X-ray Microscopy (STXM) was used to investigate the electronic structure at the interface of different regions in the samples, which were prepared at different charge and discharge states based on Cyclic Voltammetry (CV). Among the samples with varying weight ratios, 1.6NiCo-20cy showed better electrochemical properties and charge storage capacity than the others. Therefore, this sample was subjected for *ex-situ* STXM to gain a deeper understanding of the electrochemical reaction mechanism.

Figure 1 displays the optical density images and corresponding stack-mapped STXM images for the O K-edge for the as-prepared 1.6NiCo-20cy sample (Fig. 1(a)), as well as those following full charging (Fig. 1(b)) and full discharging (Fig. 1(c)). Notably, two predominant regions, A and B, bisected at 535 eV are observed. In the region A, at around 532.8 eV is attributed to π* transitions, which are strongly associated with the chemical environment of the oxygen bonds, and resulted from C=O and/or O-C–O π* transitions. The region B mainly correspond to the σ* transitions, attributed to a mixed O-H, C-O, or C=O states. A significant variation in the π* state is clearly observed, indicating its critical role in charge storage performance.

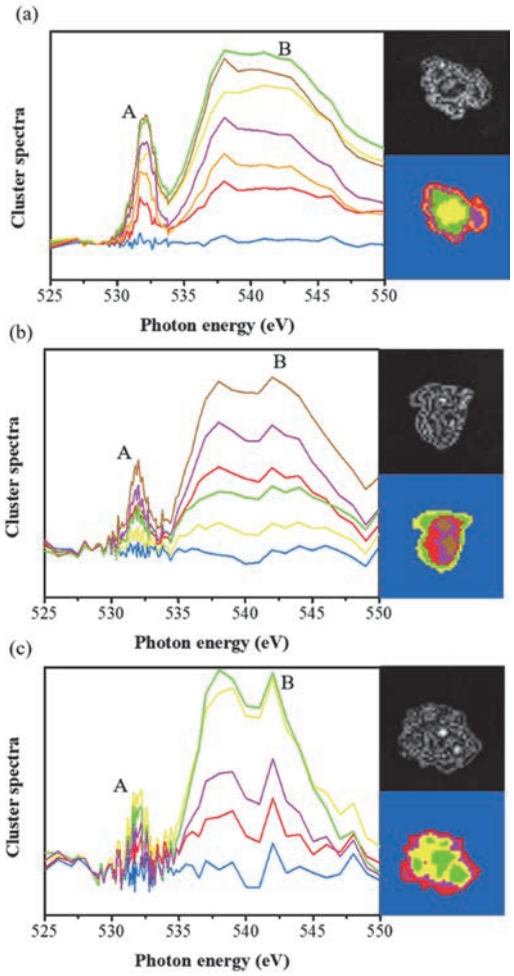

Fig. 1. Optical density images, stack-mapped STXM images, and the corresponding O K-edge XAS of (a) 1.6NiCo-20cy-Pristine, (b) fully charged-1.6NiCo-20cy and (c) fully discharged-1.6NiCo-20cy, focused at different sites of interest.

[1] T. Wang *et al.*, Nat. Commun. **14** (2023) 4607.
[2] M. Kuang *et al.*, Adv. Funct. Mater. **28** (2018) 1804886.

BL4U

Operando Nano-Scaled Identification to Carbon Dioxide and Water Gas Adsorption Coupling to Fe_3O_4 and Reduced Graphene Oxide

J. S. D. Rodriguez[1,2], H. Z. Lu[1], H. Yuzawa[3], T. Araki[3] and C. H. Chuang[1]

[1]*Department of Physics, Tamkang University, Tamsui, New Taipei City 251301, Taiwan*
[2]*Institute of Chemistry, Leiden University, Leiden 2300 RA, The Netherlands*
[3]*Institute for Molecular Science, Okazaki 444-8585, Japan*

III-2

Graphene oxide (GO)-based membranes have shown excellent CO_2 gas separation performance due to the enlargement of the interlayer distance and chemical reactivity that provide a wiggle room on physical selectivity and chemical reactivity. On the other hand, Fe_3O_4 nanoparticles (NPs), aside from their apparent high surface area innate to their structure, have good reactivity towards CO_2 chemisorption due to their electron-donating nature. Hence, intercalating Fe_3O_4 NPs into GO membranes provides not only a straightforward combination but also a strategic method to enhance several factors: modulation of interlayer distance, increase in chemical reactivity to CO_2, and improvement of mechanical and thermal stability.

Our study aims to investigate the synergistic effects of Fe_3O_4 NP with GO in a membrane configuration, in particular the chemical change near the oxygen functional groups, via chemical mapping by scanning transmission X-ray microscopy (STXM) at C K-edge, O K-edge, and Fe L-edges. To identify the regions of interest, we select the high density/low density/absence of Fe_3O_4 NPs using the STXM obtained at the Fe 707.6 eV image, by the Fe-dependent optical density (OD) contrast. In Fig. 1 (d)-(g), the area selections in four samples marked by broken lines with labels "1", "2", and "3", correspond to areas with high density, low density, and absence of Fe_3O_4 NPs, respectively. In this report, we will limit the discussion to the assessment of the high-density areas only, where the interaction between the Fe_3O_4 NPs and GO flakes is assumed to be at the greatest extent in four samples.

The oxygen functional groups (C-OH at 286.5 eV and C=O of COOH at 288.5 eV) are commonly found in DC GO-Fe_3O_4 with/without CO_2 in Fig. 1(c), assigned based on our previous pure DC GO[1]. Regarding F_3O_4 NP contribution, the high increases of C=O of COOH/C-OH at 289.7 eV and C-O of COOH/O-C(O)-O state at 290.1 eV are notable in Fig. 1(c) and our paper before[1]. The electrochemically-reduced GO (EC-rGO), when evaluated without CO_2, reveals a typical C=C bond at 285.2 eV and hexagonal C-C bond at 292.6 eV. Additionally, there has an emergence of C-OH bond at 286. 2 eV and C=O of COOH. However, the C-O-C bond at 287.4 eV is absent specifically in EC rGO[1] due to the involvement of additional Fe_3O_4 NPs. Adding CO_2 purging into the mixing solution, the apparent increases in C-OH, C-O-C, COOH, and O-C(O)-O state are observed in EC rGO-Fe_3O_4, hinting at strong oxidation between the GO flakes and the purged CO_2/further HCO_3 gases dissolved in the solution.

No significant change is observed between DC GO-Fe_3O_4 with and without CO_2, confirming that only Fe_3O_4 NPs has no function for carbon capture and storage. A notable CO_2 storage is achieved in EC GO-Fe_3O_4 w/ CO_2 compared to that w/o CO_2, in terms of EC-involved enhancement.

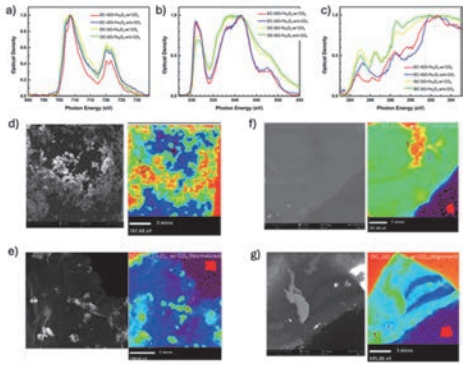

Fig. 1. (a) Fe L-edge, (b) O K-edge, and (c) C K-edge XAS spectra of EC rGO and DC GO, with and without CO_2 purging, all incorporated with Fe_3O_4 NPs. Corresponding STXM images outlining the Fe_3O_4 high-density areas of EC-rGO-Fe_3O_4 (d) w/o CO_2 and (e) w/ CO_2, and DC-GO-Fe_3O_4 (f) w/o and (g) w/ CO_2.

In the O *K*-edge (Fig. 1(b)), all samples show one π state (C=O) around 530-533.0 eV and σ state (C=O and O 2*p*-Fe 3*d*) around 537-545.0 eV, especially noted in the two DC GO-Fe_3O_4. Besides, the Fe_3O_4 characteres[2], typical of double Fe-t_{2g} and Fe-e_g states at 531.0 and 532.0 eV, are emerged in the first π peak. Through the EC method, the increase of reduced metallic states of Fe (i.e., Fe^0 and Fe^{2+}) and clear Fe 4s and 4p states become apparent at 531.0 and 545. 0 eV, respectively[2]. Compared to the only DC and EC rGO result[1], the oxygen absorption signal is dominant by the role of Fe_3O_4 NPs. No big difference is found between CO_2 purge or not. Figure 1(a) shows the Fe absorption spectra at the L_3 edge (~709.0 eV) and the L_2 edge (~722.0 eV), where they are split with the multiple crystal field and spin-orbit coupling. Two DC GO-Fe_3O_4 reveal the increasing shoulder at 707.5 eV, revealing the slight modulation of Fe_3O_4 NP after the EC method and CO_2 purge.

In summary, we exhibit the measurement of Fe_3O_4/GO composites in capturing CO_2 and the possible configurations when comparing EC rGO from DC solution, where the EC-rGO-Fe_3O_4 has shown the highest potential to capture CO_2.

[1] J. S. D. Rodriguez *et al.,* Carbon **185** (2021) 410.
[2] P.F. Teh *et al.*, J. Phys. Chem. *C* **117** (2013) 24213.

BL4U

STXM Analysis of Cathode Materials for Lithium-Ion Battery

E. Hosono[1,2], D. Asakura[1,2] and H. Yuzawa[3]

[1]*Research Institute for Energy Efficient Technologies, National Institute of Advanced Industrial Science (AIST), AIST Tsukuba Central 5, 1-1-1 Higashi, Tsukuba, Ibaraki 305-8565, Japan*

[2]*Global Zero Emission Research Center, AIST, AIST Tsukuba West, 16-1 Onogawa, Tsukuba, Ibaraki 305-8569, Japan*

[3]*UVSOR Synchrotron Facility, Institute for Molecular Science, Okazaki, Aichi 444-8585, Japan*

Toward the realization of a sustainable low-carbon society, development of clean energy devices is actively underway. Secondary batteries, which can directly store renewable energy such as solar and wind power as electricity, are attracting significant attention. Lithium-ion batteries (LIBs) with high energy density are used in electric vehicles. Moreover, they are promising for large-scale stationary storage batteries. As such expanding the practical use of LIBs, it is essential to not only improve the energy density but also ensure high safety. Therefore, establishment of highly safe operation and elucidation of degradation mechanisms are of particular importance.

Among various analytical methods of LIBs, we have focused on synchrotron soft X-ray spectroscopy and conducted detailed analyses of the 3*d* transition metals and oxygen, which are the main elements of the cathode materials. Furthermore, we have also focused on microspectroscopy, which provides local spatial information and detail spatial distribution of target species. Thus, we have reported on synchrotron soft X-ray micro-electron spectroscopy using 3DnanoESCA [1-3] and synchrotron soft X-ray Scanning Transmission X-ray Microscopy (STXM) using UVSOR BL4U [4, 5].

In this study, we have applied the STXM to LIB cathode electrode sheet with active material ($LiNi_{0.5}Co_{0.2}Mn_{0.3}O_2$). The thin sample for STXM was prepared by Focused Ion Beam-Scanning Electron Microscope (FIB-SEM).

Figure 1 shows an image of a STXM sample; the LIB electrode sheets typically consist of active material, carbon as a conductive additive, and a binder. Additionally, it is known that a solid electrolyte interphase (SEI) forms on the surface of the active material in LIBs. It is anticipated that the degradation state differs between the interior and surface of the active material. In other words, the electronic/chemical states should not be uniform in each particle of the active material. Therefore, it is expected that STXM-based microspectroscopy will provide valuable knowledge.

Figure 2 shows Mn L_3-edge absorption spectrum in a region of interest for a cathode active material ($LiNi_{0.5}Co_{0.2}Mn_{0.3}O_2$). We have obtained enough quality of spectrum from this sample. We will conduct detailed analysis including mapping, and proceed toward elucidating the battery degradation mechanism.

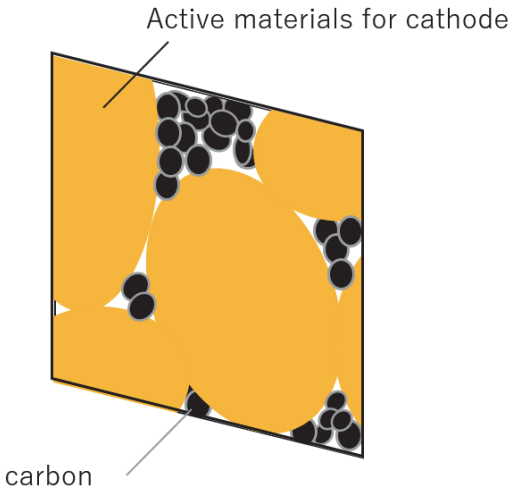

Fig. 1. Image of FIB thin section of LIB cathode electrode sheet with active material ($LiNi_{0.5}Co_{0.2}Mn_{0.3}O_2$) in STXM measurement. The structure of material is confidential until paper is published.

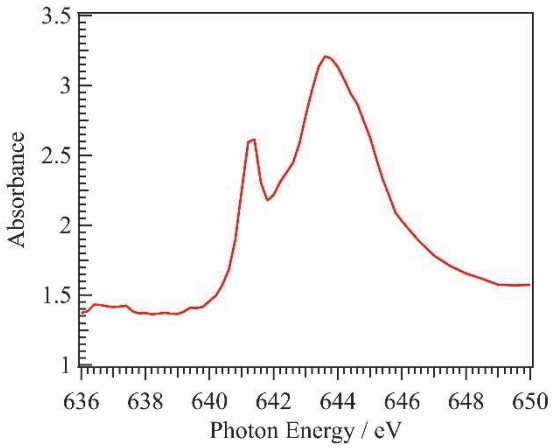

Fig. 2. Mn L_3-edge spectrum extracted from region of interest in FIB thin section of LIB cathode electrode sheet with active material ($LiNi_{0.5}Co_{0.2}Mn_{0.3}O_2$).

[1] K. Akada *et al*., Sci. Rep. **9** (2019) 12452.
[2] K. Akada *et al*., J. Electron Spectrsc. Relat. Phenom. **233** (2019) 64.
[3] W.X. Zhang *et al*., CrystEngComm. **25** (2023) 183.
[4] W.X. Zhang *et al*., Sci. Rep. **13** (2023) 4639.
[5] W.X. Zhang *et al*., J. Electron Spectrsc. Relat. Phenom. **266** (2023) 147338.

BL4U

Study of Localized Chemical State of Isoprene Rubber by STXM under Tensile-Stressed Condition

T. Ohigashi[1,2], F. Kaneko[3], H. Yuzawa[4] and H. Kishimoto[3]

[1]*Institute of Material Structure Science, High Energy Accelerator Research Organization, Tsukuba 305-0801, Japan*

[2]*Materials Structure Sciences, The Graduate University for Advanced Studies (SOKENDAI), Tsukuba 305-0801, Japan*

[3]*Sumitomo Rubber Industries Ltd., Kobe 651-0072, Japan*

[4]*UVSOR Synchrotron Facility, Institute for Molecular Science, Okazaki 444-8585, Japan*

In recent years, the Sustainable Development Goals (SDGs) have emerged as a framework guiding societal practices included in daily life. Among the various targets, the reduction of mass consumption represents a particularly critical challenge. Rubber, as a vital industrial material, is increasing its demand, especially driven by the expansion of the automobile society. In order to mitigate its consumption, it is necessary to establish a comprehensive Life Cycle Assessment (LCA) framework for rubber production, alongside the development of advanced rubber materials exhibiting enhanced functionalities, such as improved resistance to wear and mechanical failure.

A deeper understanding of the damage mechanisms in rubber materials is crucial for improving their properties. Damage in tire rubbers generally arises from a combination of chemical and mechanical factors. Recently, Mashita et al. investigated the mechanical degradation of rubber using four-dimensional X-ray tomography, revealing the creation of microvoids within deformed rubber pillars [1]. As a complementary approach aimed at elucidating the chemical aspects of mechanical damage, we have employed Scanning Transmission X-ray Microscopy (STXM). STXM enables the analysis of localized chemical states with a spatial resolution around 30 nm. Furthermore, STXM offers a relatively long working distance of ~300 μm, facilitating specialized experimental designs through the fabrication of customized sample cells. In the previous study, we developed a tensile-stress sample cell compatible with STXM and conducted *in-situ* measurements on rubber specimens [2].

An ultra-thin section (200 nm thick) of isoprene rubber was used as a sample and was attached on a tensile-stress sample grid. With changing tensile stress, 2-dimensioinal X-ray absorption spectroscopy (XAS) spectra around C K-edge (280~300 eV) were measured with 2 ms dwell time and 150 nm scanning step. Figure 1 shows the optical density images of the sample without (a, b) and with tensile stress (c, d) at 282 eV. In the tensile stress condition, the sample was stretched as 220% width for horizontal direction. Figure 1(b) and 1(d) were acquired from the same sample but at near different places to avoid radiation damage. Some bright spots in the images are considered as carbon black particles. XAS spectra under these conditions are shown in Fig. 2. Height of the spectra with tensile stress is ~52% of one without tensile stress because the sample was thinned by stretching. The main spectral change is ratio between intensity at π* (285.3 eV) and σ* (292.2 eV). The ratio (π*/σ*) changes from 0.97 to 1.12. This change is currently under discussion including formation of microvoids on the sample.

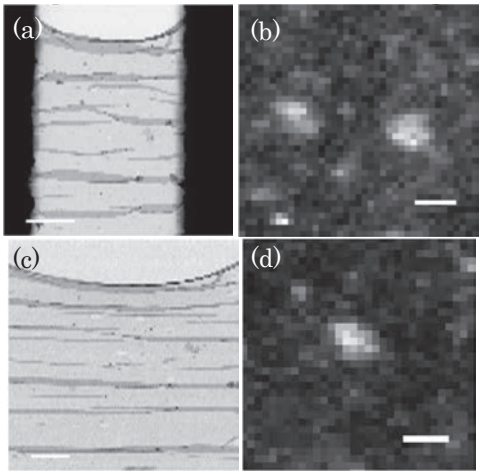

Fig. 1. Optical density images of the isoprene rubber (a, b) without and (c, d) with tensile stress at 282 eV. Scale bars are (a, c) 100 μm and (b,d) 1 μm, respectively.

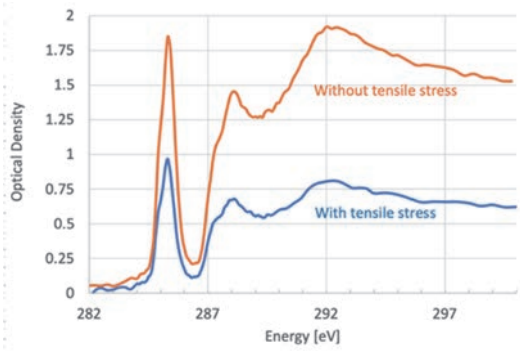

Fig. 2. C K-edge XAS spectra of the isoprene rubber without /with tensile stress.

[1] R. Mashita *et al.*, Sci. Rep. **13** (2023) 5805.
[2] T. Ohigashi *et al.*, UVSOR Activity Report **51** (2023) 84.

BL4U

Heterostructure of WO_3/V_2O_5 for Electrochromic and Energy Storage: A View by Spectro-Microscopy

K. T. Arul[1], P. C. Wang[2,1], T. Araki[3], T. Ohigashi[3,4], D. H. Wei[2] and C. L. Dong[1]

[1]*Department of Physics, Tamkang University, Tamsui 25137, Taiwan*
[2]*Graduate Institute of Manufacturing Technology, National Taipei University of Technology, Taipei 10608, Taiwan*
[3]*UVSOR Synchrotron Facility, Institute for Molecular Science, Okazaki 444-8585, Japan*
[4]*Photon Factory, High Energy Accelerator Research Organization, Tukuba 305-0801, Japan*

To address high energy consumption and related energy issues, such as low energy and power densities and stability, a combination of electrochromism and energy storage has been explored to support both energy saving and charge storage, leading to the development of electrochromic supercapacitor (ECS) devices. ECS technology can control thermal radiation, and mitigate the need for artificial lighting in buildings, enhance energy efficiency, and even power electrical systems. These devices have been applied in energy harvesting, liquid crystal displays, wearable electronic devices, etc., [1]. Several metal oxides and their nanostructures, heterostructures, and composites have been extensively studied as ECS materials [2]. Among them, vanadium and tungsten oxides are particularly promising owing to their multi-oxidation states, high electronic conductivity, redox activity, structural stability, and high optical contrast.

The fundamental understanding of the electrochromic energy storage mechanism in the heterostructure is essential. In this study, the bifunctional WO_3/V_2O_5 thin films (~150-200 nm) were prepared using the sol-gel method. The XRD analysis revealed the presence of the (001) and (020) planes, indicating the crystalline phases of V_2O_5 and WO_3, respectively. The ultraviolet-visible spectroscopy revealed that the thin film exhibited the optical switching contrast of 17.4% between bleached and colored states, with a coloration efficiency of 10.78 cm^2/C. Moreover, the specific capacitance of WO_3/V_2O_5 was 8 F/g, which is higher than that of the individual V_2O_5 and WO_3 films, demonstrating its potential as a bifunctional material for smart film and charge storage. In this work, scanning transmission X-ray microscopy (STXM) is employed to investigate the active regions and/or elements responsible for the electrochromic energy storage performance.

Figure 1 shows the optical density and corresponding stack-mapped STXM images for the V L- and O K-edge XAS of the samples. The V L-edge originates from the V 2p-to-3d unoccupied state [3]. In the WO_3/V_2O_5 heterostructure, the intensity of the V L_3-edge peak is slightly higher at surface of the heterostructure. The O K-edge XAS, which arises from O 1s-to-2p transitions hybridized with V 3d and W 5d states, was also measured. The peaks a_1 and a_4 correspond to, respectively, the O 1s-to-2p states hybridized with W 5d-t_{2g} and 5d-e_g states. The peaks a_2 and a_3 are attributed to the O 1s-to-2p states hybridized with V 3d-t_{2g} and 3d-e_g states, respectively. The spectral evolutions indicate a higher concentration of oxygen vacancies at the surface than in the core, particularly around W sites, providing more active sites for electrochromic energy storage.

In contrast, the V L- and O K-edge XAS-STXM of WO_3/V_2O_5 heterostructure after cyclic voltammetry (CV) treatment shown in Fig.1b, revealed a stronger interaction between V and W through oxygen 2p states. Notably, the charge states of both V and W are more reduced at the surface of the particle compared to the core region, suggesting that both V and W in the heterostructure are electrochemistry active. The stability of such a defective heterostructure, the durability of these active sites, and whether both active sites are jointly (or separately) responsible for the electrochromic and charge storage functionalities remain to be explored.

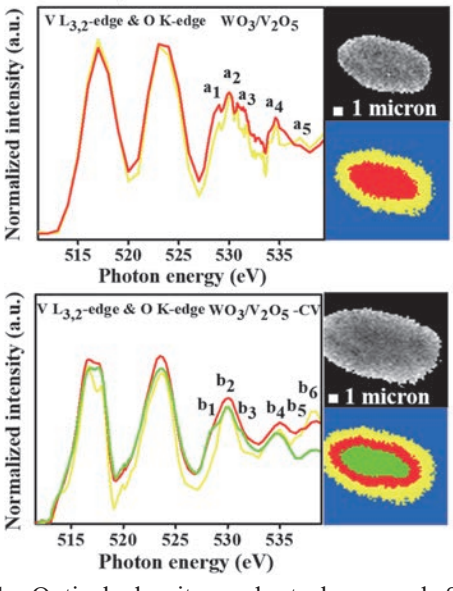

Fig. 1. Optical density and stack-mapped STXM images, and the corresponding V $L_{3,2}$- and O K-edge XAS of (a) WO_3/V_2O_5 and (b) WO_3/V_2O_5-CV.

[1] D. K. Pathak *et al.*, Mater. Horiz. **9** (2022) 2949.
[2] S. Zhang *et al.*, Energy Environ. Sci. **11** (2018) 2884,
[3] Q. Lu *et al.*, Adv. Funct. Mater. **28** (2018) 1803024.

BL4U

Scanning Transmission X-ray Microscopy (STXM) Study of Co Oxidation State Evolution in Nano- and Micro-Sized $LiCoO_2$ During Alkaline OER

Y. Zhang[1], J. Lei[1], T. Araki[2] and J. Wang[1]
[1]*City University of Hong Kong, Kowlong, Hong Kong*
[2]*UVSOR Synchrotron Facility, Institute for Molecular Science, Okazaki 444-8585, Japan*

Layered $LiCoO_2$ (LCO), well-known as a cathode in lithium-ion batteries, also shows promise as an alkaline oxygen evolution reaction (OER) electrocatalyst due to its $Co^{3+}\leftrightarrow Co^{4+}$ redox activity and robust Co–O framework [1]. Studies have demonstrated that Na^+ or K^+ incorporation in LCO can enhance Co–O covalency, boosting OER activity while preserving structural integrity [2]. Nanoscale LCO, in particular, offers abundant Co^{3+}-rich surface facets and favorable electronic structures for redox kinetics. Conversely, micro-sized LCO (mLCO) often suffers from limited lithium diffusion, surface Co dissolution, and structural reconstruction under prolonged OER conditions [3,4].

To explore how particle size influences Co valence state distribution during OER, we performed STXM with Co L_3-edge XANES on nanoparticulate LCO (nLCO, ≈ 50 nm) and micron-sized LCO (mLCO, ≈ 1 μm). Samples were polarized in 1 M KOH at 1.5 V vs. RHE for 10 min and 30 min. We aimed to determine: (i) initial oxidation homogeneity, (ii) short-term oxidation evolution, and (iii) spatial heterogeneity after prolonged exposure.

STXM maps of pristine samples showed that nLCO consistently exhibited an XANES peak at 778.0 eV, indicating a homogeneous Co^{3+} oxidation state (Fig. 1a). In contrast, mLCO displayed a broader peak around 776.8 eV, signifying mixed Co^{2+}/Co^{3+} states and a lower overall oxidation level (Fig. 1b). The enhanced surface energy and electronic coupling in nLCO likely stabilize Co^{3+}, consistent with previous findings on size-dependent structural robustness [1, 3].

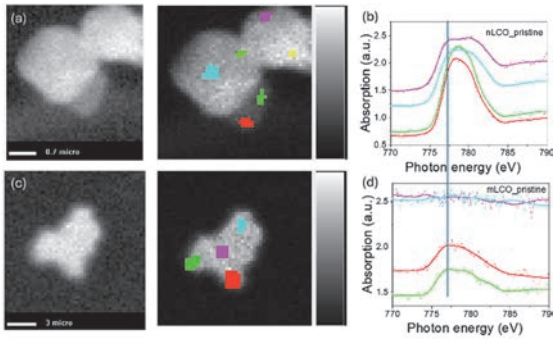

Fig. 1. STXM of nLCO pristine (a-b) and mLCO pristine (c-d).

After 10 minutes of OER polarization, the Co peak in nLCO slightly shifted to ~777.8 eV but remained indicative of Co^{3+} (Fig. 2a). Remarkably, mLCO's peak shifted from 776.8 to ~777.9 eV (Fig. 2b), aligning with nLCO. This reveals rapid oxidation of surface Co^{2+} to Co^{3+} in mLCO, demonstrating that even micro-sized particles can achieve surface valence homogenization under short-term OER conditions.

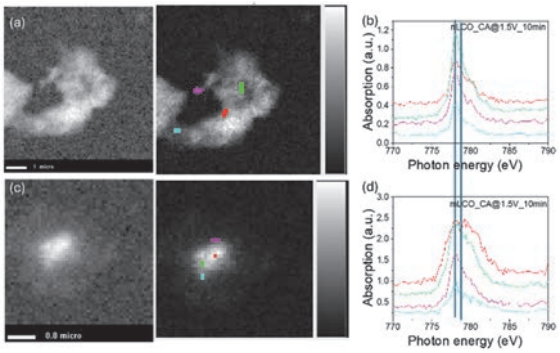

Fig. 2. STXM of nLCO (a-b) and mLCO (c-d) after CA at 1.5V for 10min.

Prolonged polarization showed divergent trends: nLCO retained uniform Co^{3+} distribution with no spatial variation (Fig. 3a) while mLCO developed clear spatial heterogeneity—edge regions exhibited peaks at ~778.0 eV (possibly over-oxidized Co^{3+}), while core areas remained around ~777.8 eV (Fig. 3b). This behavior results from rapid edge oxidation by OH^- and slower lithium deintercalation in the core, leading to non-uniform internal oxidation—a phenomenon observed in larger LCO crystals [4].

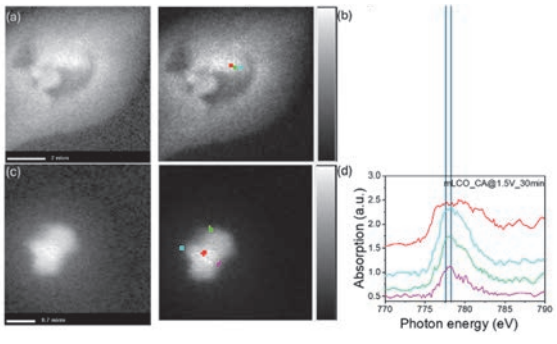

Fig. 3. STXM of nLCO (a-b) and mLCO (c-d) after CA at 1.5V for 30min.

[1] Y. Kim *et al.*, J. Mater. Chem. A **10** (2022) 10967.
[2] J. Qian *et al.*, Nat. Commun. **9** (2018) 4918.
[3] Y. Kim *et al.*, J. Phys. Chem. Lett. **6** (2015) 1357.
[4] T. Maiyalagan *et al.*, Nat. Commun. **6** (2015) 3949.

BL4U

In Situ STXM-Based Approach to Visualize Polymer Fracture: Demonstration with Polystyrene

T. Ejima[1,2], E. Sasaki[2] and Y. Tamura[3]
[1]*SRIS &* [2]*IMRAM, Tohoku University, Sendai 980-8577, Japan*
[3]*ENEOS Materials Corp., Yokkaichi 510-0871, Japan*

Polystyrene (PS) is a widely used thermoplastic owing to its low cost, high transparency, and ease of processing. The fracture behavior of PS is primarily attributed to main-chain scission, in which carbon–carbon bonds within the polymer backbone are ruptured—a phenomenon widely observed in polymeric systems. Although molecular probes such as fluorescent dyes and stabilized radicals have facilitated the visualization of such events, methods for directly detecting main-chain scission remain limited [1].

Carbon K-edge spectral imaging at sub-micron resolution is expected to reveal stress-induced electronic structural changes and elucidate fracture mechanisms, with a particular focus on main-chain scission [2]. The objective of this study is to visualize polymer fracture without the use of dyes or radicals by performing in situ stress-application experiments using scanning transmission X-ray microscopy (STXM). To this end, a custom-designed sample holder was developed by integrating the STXM frame from BL4U (UVSOR) with a cartridge designed for simultaneous tensile deformation and TEM observation [3]. The holder incorporates a piezo-linear actuator (Picomotor™, Model 8302, Newport) connected to a lever, enabling precise displacement control (Fig. 1a). The cartridge contains a flexure structure that is actuated by the lever, thereby applying stress to the sample (Fig. 1b). Polymer samples were mounted on parallel TEM grids and secured with double-sided adhesive tape. The conversion of vertical lever motion into horizontal displacement resulted in an opening displacement of 9.02 ± 0.18 nm per actuator pulse.

The measurements were conducted using injection-grade polystyrene (HF77, PS Japan Corporation), which was sectioned into 100 nm-thick slices using an ultramicrotome. These slices were mounted on TEM grids (40 μm bar width, 62 μm pitch) and affixed to the cartridge. During STXM, soft X-rays from the BL4U monochromator were focused to a 50 nm spot using a zone plate. The images were acquired with a pixel exposure time of 2 ms.

Two stress-application measurements were conducted, both showing PS fracture at strain levels between 0.327 and 0.460. Below 0.327, the STXM spectra from the PS region exhibited consistent profiles (Fig. 2) corresponding to previously reported PS spectra [2]. Normalized absorption spectra revealed a strain-dependent increase near 285 eV (inset of Fig. 2), consistent with π* orbitals from benzene rings [2, 4], indicating alignment of the ring along the X-ray direction [4]. These results suggest that stress-application STXM offers enhanced potential for elucidating polymer fracture mechanisms.

Acknowledgement:
The authors thank the Machine Shop of IMRAM, Tohoku University for their support in fabricating the STXM holder.

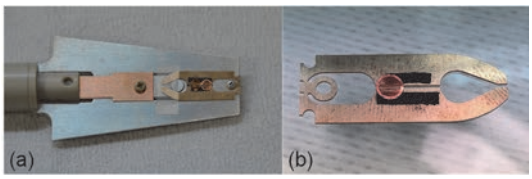

Fig. 1. (a) STXM holder frame with a piezo-linear actuator, (b) Sample cartridge: Stress is applied to the sample by opening and closing the flexure structure.

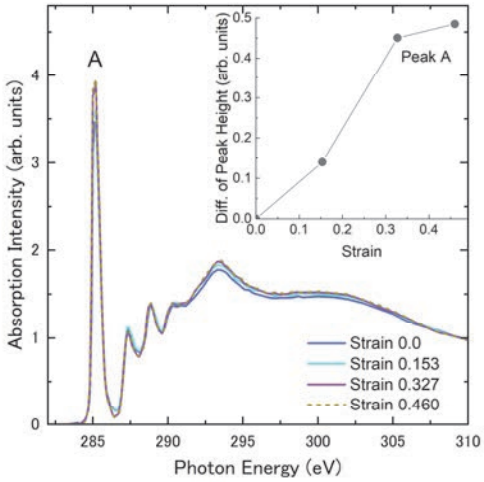

Fig. 2. Spectral shape the major area is the same of PS [2]. Inset is the intensity change of peak A.

[1] T. Yamamoto, D. Aoki and H. Otsuka, ACS Macro Lett. **10** (2021) 744.
[2] J. Stöhr, *NEXAFS Spectroscopy* (Springer, Berlin & Heidelberg, 1992) §7.4, p.230.
[3] T. Higuchi *et al*., Microscopy **67** (2018) 296.
[4] J. A. Horsley *et al*, J. Chem. Phys., **83**(12) (1985) 6099.

BL4U

X-ray Absorption Spectroscopic Analysis of Spatial Distribution of Water Molecules in Deep-Sea White Smoker Chimney Minerals

H. E. Lee[1], T. Araki[2] H. Takahashi[1], and A. Koishi[3]
[1]*Editorial Board, Earth-Life Science Institute (ELSI), Institute of Science Tokyo, Tokyo 152-8550, Japan*
[2]*UVSOR Synchrotron Facility, Institute for Molecular Science, Okazaki 444-8585, Japan*
[3]*RIKEN Center for Sustainable Resource Science, Wako, Saitama 351-0198 Japan*

This study successfully conducted the world's first spatially-resolved soft X-ray absorption spectroscopy (STXM) analysis on minerals collected from the White Smoker Chimney located in the Mariana Trench (depth: 5743 meters)[1]. The primary aim was to investigate the chemical state and two-dimensional spatial distribution of water molecules within the nano-confined spaces of $Mg(OH)_2$ based mineral structures that constitute the chimney. Utilizing the oxygen K-edge spectra, the measurements allow us to map the presence and orientation of water molecules under both dry and humidified conditions.

Our findings reveal that water confined in the nanoscale environments created by oriented $Mg(OH)_2$ exhibits distinct molecular orientations and hydrogen bonding characteristics that differ markedly from bulk water. These altered properties are critical because they suggest the possibility of facilitating dehydration-condensation reactions, such as those involved in the formation of peptides or nucleic acids, which are generally inhibited in bulk aqueous environments. This insight directly addresses the long-standing "Water Paradox" in the origin of life research, where water is essential for life but simultaneously suppresses key synthetic reactions[2].

By employing a soft X-ray beam at BL4U (UVSOR), the study achieved high resolution in visualizing the distribution of water at the nanoscale in a wet environment. The spectroscopic features observed in the pre-edge (~535 eV), main-edge (~537 eV), and post-edge (~540 eV) regions provided detailed information on the saturation level of hydrogen bonds and surface interactions. An increased peak intensity was observed around 536~537 eV, which is expected to be associated with the characteristics of confined water[3].

As only a few research groups worldwide possess samples from the White Smoker Chimney, the structural and chemical insights provided by this study are both novel and significant. The experimental techniques developed and applied here offer a powerful platform for future exploration of water–mineral interactions and their role in supporting life-like chemical processes in extreme environments. This research not only opens new avenues in catalytic chemistry by highlighting the functional potential of mineral-bound nano-confined water but also contributes fundamentally to the field of prebiotic chemistry and the study of life's origins.

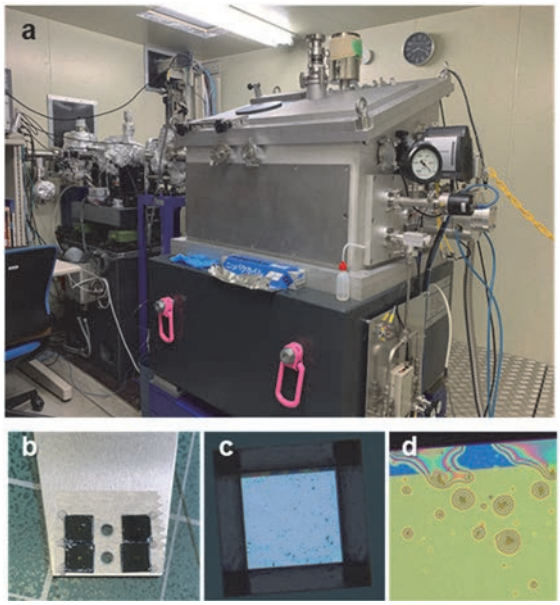

Fig. 1. a. Photograph of the STXM setup at UVSOR. b. Wet cell mounted on the sample holder. c, d. Samples enclosed within a wet cell, prepared by sandwiching them between two SiNx windows.

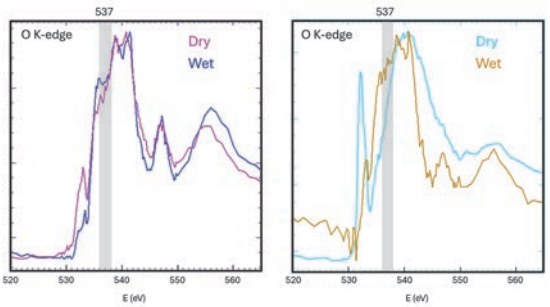

Fig. 2. O K-edge spectra of two different samples with wet and dry conditions.

[1] H.-E. Lee *et al.*, Nat. Commun. **15** (2024) 8193.
[2] M. Marshall, Nature **588** (2020) 210.
[3] K. Yamazoe *et al.*, Langmuir **33** (2017) 3954.

BL4U

Nocturnal Aerosol Growth in New Delhi – A Microscopic Investigation

M. Wickramanayake[1], E. Tsiligiannis[1], T. Araki[2] and X. Kong[1]
[1]*Department of Chemistry and Molecular Biology, University of Gothenburg, SE-412 96 Gothenburg, Sweden*
[2]*UVSOR Synchrotron, Institute for Molecular Science, Okazaki 444-8585, Japan*

This study explores the nighttime growth of atmospheric aerosol particles in New Delhi, one of the most polluted megacities globally, using advanced synchrotron-based techniques. The research addresses a significant knowledge gap in understanding the molecular composition and growth mechanisms of aerosols [1], particularly during nocturnal hours in winter when air pollution events intensify [2]. Sampling was conducted in February and March 2023 from the rooftop of the Indian Institute of Technology (IIT) Delhi, and analytical measurements were carried out at the UVSOR-III synchrotron facility in Japan in March 2024. The primary tools used were Scanning Transmission X-ray Microscopy (STXM) and Near Edge X-ray Absorption Fine Structure (NEXAFS) spectroscopy, enabling high-resolution imaging and chemical speciation of individual aerosol particles.

This investigation examines the diurnal variation of aerosol particle morphology and composition in New Delhi using STXM images at 300 eV, an energy optimal for detecting carbonaceous materials. Three particle types were identified by color: black (carbon- rich soot), grey (inorganics like potassium), and mixed (organic-inorganic combinations). Black particles often appeared chain-like, grey ones polygonal, and mixed particles suggested internal mixing due to condensation or fog processing.

Figure 1 captured during four different conditions (polluted day, clean day, polluted night, and clean night) show significant changes in particle abundance and morphology. Notably, the nighttime images showed a higher degree of spherical structures and internal mixing, supporting the idea of aqueous-phase processing under high humidity conditions, which is common at night in winter.

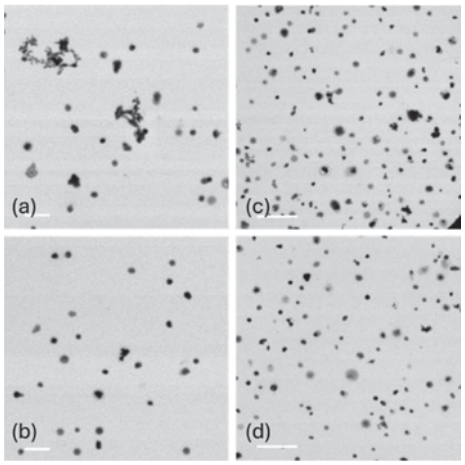

Fig. 1. STXM images of particle morphology during (a) polluted day, (b) clean day, (c) polluted night, and (d) clean night. The scale bar of each is in the bottom left corner showing as a white strip, where (a) and (b) are 2 μm, (c) and (d) are 5 μm.

A key observation lies in the change in particle composition. During both night conditions, the proportion of mixed particles increased, while the number of black (carbonaceous) particles decreased. In the polluted scenario, mixed particles increased by 13%, while black particles dropped by 8% and grey particles by 5%. For the clean scenario, the increase in mixed particles was even more prominent (15%) while grey particles rose by 13%, and black particles showed a sharp 28% decline. This suggests that nighttime conditions favor the transformation of pure carbonaceous or inorganic particles into more internally mixed forms, likely due to condensation of organic vapors and moisture.

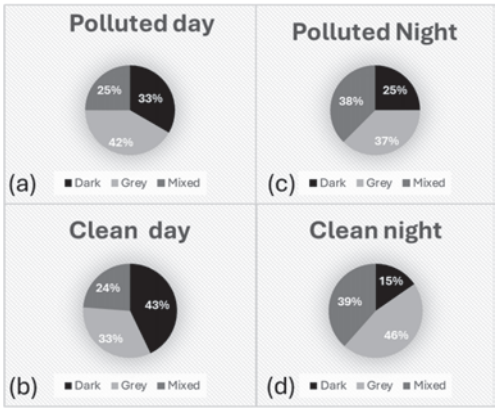

Fig. 2. The fractions of particles distributed into three categories.

The mixing state, which influences how particles interact with solar radiation and water vapor, shifts notably at night. The presence of internally mixed, spherical particles suggests fog or aqueous-phase processing, where particles absorb or coat one another, altering their chemical composition. This affects both climate forcing and health, as internally mixed particles have different optical and hygroscopic properties than externally mixed ones. STXM image analysis and particle count data show that nighttime conditions in New Delhi led to more internally mixed aerosols with larger sizes and distinct compositions. These changes are driven by lower temperatures, higher humidity, and emissions from biomass burning. The results underscore the need to consider diurnal variation in air quality assessments and control strategies.

[1] M.Hallquist *et al.*, Atmos. Chem. Phys. **9** (2009) 5155.
[2] J. K. Kodros *et al.*, PNAS **117** (2020) 33028.

III-5

BL4U

Trial of Molecular Mapping for Thin Sections of Isolated Mammalian Nuclei Embedded in Paraffin Using STXM

A. Ito[1], K. Shinohara[2], A. Matsuura[2], S. Toné[3], S. Ohira[4], A. Nagai[4], Y. Asada[2], T. Ohigashi[5], H. Yuzawa[6] and T. Araki[6]

[1]*School of Engineering, Tokai University, Hiratsuka 259-1292, Japan*
[2]*Graduate School of Health Sciences, Fujita Health University, Toyoake 470-1192, Japan*
[3]*School of Science and Engineering, Tokyo Denki University, Hatoyama 350-0394, Japan*
[4]*Kawasaki Medical School, Kurashiki 701-0192, Japan*
[5]*Photon Factory, Institute of Materials Structure Science, Tsukuba 305-0801, Japan*
[6]*UVSOR Synchrotron Facility, Institute for Molecular Science, Okazaki 444-8585, Japan*

Spectromicroscopy using STXM is one of the most effective tools for molecular mapping at high spatial resolution. For the application to biological specimens, we have developed an image processing method for a quantitative distribution of constituent molecules, and successfully obtained molecular images in chromosomes, mammalian cells, and mammalian isolated normal and apoptotic nuclei [1-3]. However, due to low transmission of soft X-rays to thick areas in the isolated nucleus, reliable analysis for molecular distribution could not be achieved [3]. To try to solve this problem, thin sections of isolated nuclei with the thickness around 200 nm were prepared by embedding in resin [4]. Although the transmission was greatly improved, we could not exclude the possibility that significant amount of resin in the sections might interfere in the analysis for molecular distribution. In the present study, we adopted paraffin in place of resin, because paraffin in the thin section can be removed by soaking in xylene. In contrast, paraffin section is not so thin as resin section; around 2 μm thickness would be lower limit of the thickness. This report is the first preliminary results using paraffin embedded section.

Isolated nuclei from human HeLa S3 cells were fixed with glutaraldehyde followed by mixing with agarose to confine to a limited volume, and then embedded in paraffin. The paraffin sections were prepared with thicknesses of 5, 3 and 2 μm, and found that 2 μm was the best choice from the transmitted intensity. The section was attached directly on SiN membrane and then soaked in xylene to remove paraffin from section samples.

We basically applied the SVD (Singular Value Decomposition) method to obtain molecular distributions [3]. Energy stack images obtained at the C, N and O-K edges were analyzed using NEXAFS spectra of nucleic acids (DNA and RNA), proteins (histone and actin), and agarose.

Figure 1a shows an X-ray transmission image of a 2 μm-thick thin section of an isolated nucleus observed at 285 eV, where the dense area in the center of nucleus may be assigned to be a nucleolus. The image has somewhat irregular jagged boundary, which may result from sectioning technique of challenging thin thickness. Molecular images of DNA, RNA, histone, and actin were shown in the same OD scale for quantitative comparison, in the panel b, c, d, and e, respectively. RNA is likely to be localized in the nucleolus. Actin is known as one of nuclear proteins as well as cytoplasmic cytoskeletal protein. Although the present analysis is preliminary, because residual molecules are found to exist with significant quantity, the result indicated that the present preparation of the thin section with paraffin for imaging nucleus will be successful. Analysis including paraffin spectra is in progress.

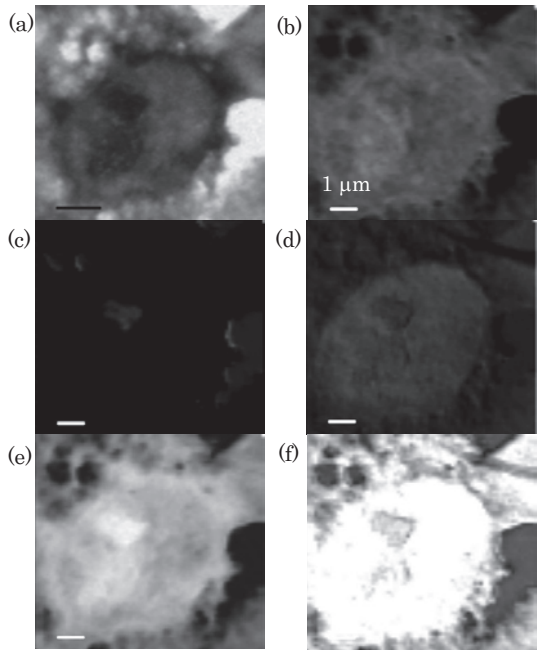

Fig. 1. Molecular distributions in an isolated human nucleus. (a) X-ray image at 285 eV, (b-e) molecular distribution of DNA, RNA, histone and actin, (f) residual molecules.

[1] K. Shinohara *et al*., Ultramicrosc. **194** (2018) 1.
[2] K. Shinohara *et al.*, J. X-Ray Sci. Technol. **26** (2018) 877.
[3] K. Shinohara *et al.*, Cells **8** (2019) 164.
[4] A. Ito *et al*., UVSOR Activity Report **48** (2020) 130.

BL4U

Investigation of the Terrestrial Weathering Process of Ryugu Grains

M. Miyahara[1] and T. Araki[2]

[1]*Graduate School of Advanced Science and Engineering, Hiroshima University, 1-3-1 Kagamiyama, Higashi-Hiroshima, Hiroshima 739-8526, Japan*

[2]*UVSOR Synchrotron Facility, Institute for Molecular Science, Okazaki 444-8585, Japan*

Ryugu grains, which are collected from the asteroid Ryugu, mainly consist of saponite, serpentine, magnetite, sulfides, carbonates, and phosphates, closely resembling CI-group carbonaceous chondrites [1]. CI chondrites are highly susceptible to terrestrial weathering, making it difficult to study their original features. Even Antarctic meteorites, despite better preservation, experience long exposure to water and ice. To understand early-stage terrestrial weathering of CI chondrites, this study proposes to expose Ryugu grains to atmospheric conditions and monitor surface changes, providing insights into weathering processes not possible from meteorites alone.

The sample plate C0105-042, previously analyzed by the Hayabusa2 Initial Analysis "Sand" Team, was used in this study [2]. It contains small Ryugu grains from chamber C of the second touchdown. After allocation by JAXA, over 24 grains were mounted onto C0105-042 with minimal epoxy in an N_2-filled glove box. Following approval of our terrestrial weathering AO proposal, the sample plate C0105-042 was sent to Hiroshima University. The sample plate C0105-042 was exposed to air in a desiccator. FE-SEM observations were done 104 and 245 days after exposure began. For TEM and STXM analysis, ultrathin foils were prepared using a FIB system. TEM observations and SAED pattern analysis were conducted for structural and chemical analysis, with quantitative EDS analysis. STXM analysis was conducted at BL4U, UVSOR Synchrotron facility to analyze C K-, S L-, and Fe L-edges using energy stacking methods. Elemental maps and NEXAFS spectra were processed using aXis2000.

FE-SEM observations of the C0105-042 Ryugu grains showed significant surface changes after exposure experiments. Cracks widened, some grains fragmented, and fine-grained precipitates (Fig. 1a) formed on mineral surfaces. Pyrrhotite surfaces were entirely covered by amorphous, amoeboid precipitates (Fig. 1b), obscuring their original outlines. With longer atmospheric exposure, precipitate sizes increased (>200–300 nm), and cracked grains detached completely. TEM analysis revealed that these precipitates were mostly amorphous, carbon- and oxygen-rich layers about 100 nm thick. The amoeboid precipitates on pyrrhotite were iron- and sulfur-depleted, oxidized or hydrated.

Based on the Fe L_3-edge XANES spectra, Fe^{2+} is dominant in the pyrrhotite ($Fe_{1-x}S$)-dominated regions, whereas Fe^{3+} is dominant in the saponite–serpentine matrix. S L-edge XANES spectrum indicate that at pyrrhotite-dominated regions, minor absorption peaks appear around 162 eV and 164 eV (Fig. 1c), corresponding to S^{2-} and elemental sulfur (S^0), respectively [3, 4]. Additionally, a broad absorption band between 167–174 eV is observed (Fig. 1c), attributed to oxidized sulfur species such as S^{4+} and S^{6+} [4]. C K-edge XANES spectrum show that at saponite–serpentine matrix that include carbonaceous material an absorption near 290.5 eV is observed, corresponding to carbonate (CO_3^{2-}) groups [5]. The absorption peak corresponding to the carbonate becomes weaker and an absorption peak corresponding to the C=C bond appears instead as the fine-grained precipitate layer is close to the surface of minerals

Considering the TEM observations and STXM analysis, the terrestrial weathering of Ryugu grains is initiated by the natural oxidation of pyrrhotite. It is highly probable that pyrrhotite reacts with atmospheric moisture, leading to the oxidation of sulfur into sulfate ions, which in turn may cause the decomposition of surrounding saponite, serpentine, and carbonaceous materials. The mechanism and rate by which sulfur leached from pyrrhotite affects these adjacent materials are currently under investigation.

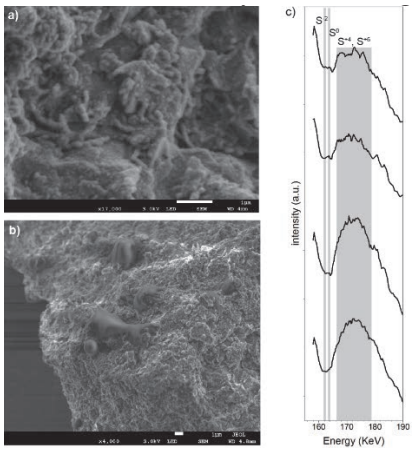

Fig. 1. SE images of a) fine-grained precipitates and b) amoeboid precipitates and c) Representative S L-edge XANES spectrum.

[1] T. Nakamura *et al*., Science **379** (2023) eabn8671.
[2] T. Noguchi *et al*., Nat. Astron. **7** (2023) 170.
[3] S. P. Farrell *et al*., Am. Mineral. **87** (2002) 1321.
[4] D. Li *et al*., Can. Mineral. **33** (1995) 949.
[5] J. A. Brandes *et al*., J. Synchrotron Radiat. **17** (2010) 676.

BL4U

Inorganic Nitrogen in Springtime Aerosol Particles over the Arctic Ocean

N. Fauré[1], T. Araki[2], R. Pohorsky[3], G. P. Freitas[4], J. Schmale[3], P. Zieger[4], J. Creamean[5], E. S. Thomson[1] and X. Kong[1]

[1]*Department of Chemistry and Molecular Biology, University of Gothenburg, Gothenburg SE-412 96, Sweden*
[2]*UVSOR Synchrotron, Institute for Molecular Science, Okazaki 444-8585, Japan*
[3]*Extreme Environments Research Laboratory, EPFL, Sion 1950, Switzerland*
[4]*Department of Environmental Science, Stockholm University, Stockholm SE-106 91, Sweden*
[5]*Department of Atmospheric Science, Colorado State University, Fort Collins CO 80523, USA*

The Arctic region is warming at a rate two to four times faster than the global average, a phenomenon known as Arctic Amplification (AA). Aerosol particles play an important role in this accelerated warming. However, the extent of their impact depends on their physicochemical properties (e.g., chemical composition, size, and hygroscopicity). [1] Here, we utilize STXM/NEXAFS to investigate the chemical composition of both ambient and laboratory-generated Arctic springtime aerosol particles. These aerosol particles were collected during the Atmospheric Rivers and the Onset of Sea Ice Melt (ARTofMELT) expedition, which took place in the Fram Strait from May to June 2023 onboard the Swedish icebreaker Oden. Ambient aerosol particles were collected at surface level (at sea ice edge) and in clouds at higher altitudes (with a tethered balloon). Laboratory-generated aerosol particles were produced using a Sea Spray Chamber (SSC) onboard the vessel, which was filled with freshly collected seawater and melted snow.

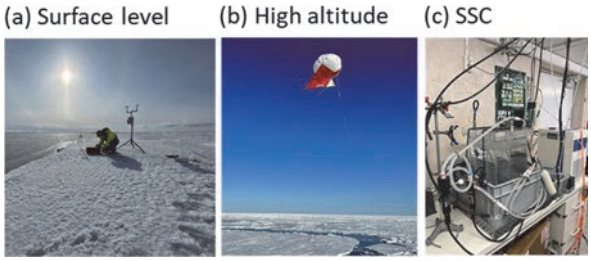

Fig. 1. Ambient aerosol particles collected (a) at the sea ice edge, (b) with a tethered balloon, and (c) from a SSC used to generated sea spray aerosol particles.

The STXM/NEXAFS results reveal that ambient aerosol particles are dominated by ammonium sulfate ($(NH_4)_2SO_4$) and sodium nitrate ($NaNO_3$), while the laboratory-generated sea spray aerosol particles are dominated by sodium chloride (NaCl). The discrepancy between the ambient aerosol particles and those generated using the SSC highlights the potential influence of different sources and formation mechanisms in the ambient environment. Notably, no chloride was detected in ambient particles, suggesting an impact of aging processes on sea spray aerosol compositions, such as dichlorination via acid replacement with nitric acid (HNO_3) and the emission of hydrogen chloride (HCl). [2] Further analysis will be conducted to better understand the different sources and mechanisms at play.

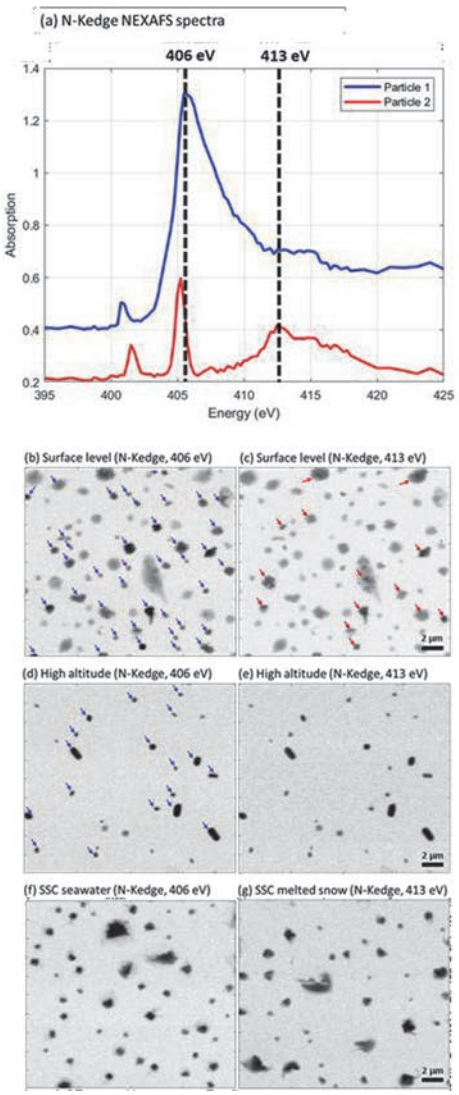

Fig. 2. (a) Nitrogen K-edge NEXAFS spectra with ammonium absorption edge (406 eV) and nitrate absorption edge (413 eV). Overview scans for particles collected (b-c) at surface level close to the sea ice edge, (d-e) at higher altitudes in cloud with a tethered balloon, (f) with the seawater filled SSC and (g) from the SSC filled from melted snow. Blue arrows correspond to particles containing ammonium, red arrows to particles containing nitrate and no arrows to particles with other compositions.

[1] J. Schmale *et al.*, Nat. Clim. Change. **11** (2021) 95.
[2] B. Su *et al.*, Atmos. Environ. **290** (2022) 119365.

BL4U

Investigating Ti-organometallic Complexes Found in Mars-relevant Mineral- microbial Interfaces Exposed Outside the ISS as Potential Biosignatures in the Search for Life on Mars

M.C. Sforna[1] and T. Milojevic[1]
[1]*Center of Molecular Biophysics, CNRS – University of Orleans, Orleans, France*

Searching for traces of life is the core of Mars exploration as conditions were reunited on early Mars for the appearance of Life. Chemolithotrophs (rock-eating microorganisms) may have been predominant on early Mars [1], but the understanding of their putative biosignatures in Martian materials is limited. We investigated *Metallosphaera sedula*, an ancient extremophilic archeon that extracts energy from diverse inorganic electron donors, and which has the particularity to induce specific biomineralization patterns depending of the substrate, which may be preserved for billions of years [2, 3]. *M. sedula* cells were grown on the 4.5 Gyrs-old NWA7034 meteorite [2], and exposed for one year outside of the International Space Station under Martian conditions within the framework of the Japanese Tanpopo-4 orbital project [4, 5]. Preliminary analyses on the retrieved cells showed that despite the abundance of Ti-oxides in NWA7034 [6], there were no traces of Ti- oxides after microbial growth, both in the exposed and in the ground control samples, ruling out photoionization processes. This transformation of Ti- oxides is intriguing, as Ti-oxides are known to be excellent catalyzers for chemical reactions, but, there are no reports of their role on bioprocesses [7]. One question arose from these results: could Ti- organometallic compounds be a suitable signature for the search of life on Mars?

To answer this question, we performed, in May and in October 2024, STXM and XANES spectroscopy at C K-edge, N K-edge, S L-edge and Ti L-edge on the BL4U beamline on exposed and ground control (GC) cells to (1) confirm that Ti accumulation in close proximity with cells is really an organometallic compound, (2) better identify the organometallic complex(es), (3) understand if this complex is preserved under Martian conditions by comparing ground control and ISS-exposed cells, and then to (4) assess Ti-organometallic complexes as potential biosignatures.

In May 2024, we investigated 2 ultra-thin sections of IS cells and ultra-thin section of GC cells, embedded in epoxy resin and deposited on TEM grids. We performed 176 images at the C K-edge and the Ti L- edge, and 25 scans in energy across the C K-edge and the Ti L-edge. In October 2024, we analyzed cells directly dropped on Si3N4 windows (4 windows for ISS, 2 for GC), and were able to better examine the change on the cells resulting from spatial exposure. We performed 141 images at the C K-edge, N K-edge, S L-edge and Ti L-edge, and 47 energy scans, mostly across the C K-edge and the S L-edge.

STXM and XANES at the Ti L-edge did not evidence the presence of Ti-organometallic compounds, but only showed the presence of nanophases of anatase and rutile associated to the cells, suggesting that the transformation of Ti-minerals is not as complete as previously thought.

Our experiment also allowed to investigate the damages on the molecular composition of the cells underwent during ISS exposition. The C K-edge spectra for GC cells show three main bands centered at ~285.1, 287.6 and 288.5 eV, indicating a mixture of biomolecules within *M. sedula*, with prominent lipids, proteins and saccharides features, with a particularly high lipid contribution compared to general composition of cells [8]. Overall, a higher hydroxylation of the functional groups can be observed in the ISS exposed cells compared to GC cells, supported by a globally stronger carboxylic signal, more defined hydroxylated aliphatic peak and carbonyl peaks, and weaker bands for the ketone/phenol/nitrile absorption region. The S L-edge spectra performed on GC and in exposed cells show similar spectra with two main bands, centered at ~173 and ~182 eV spectra, suggesting a +6 redox state for S, most certainly contained in sulphates [9], suggesting a good preservation of the sulfates. The higher hydroxylation is a common features in cells when exposed to UV. Indeed, UV radiation is known to be damageable for cells, increasing the amount of reactive oxygen species in the cells and hydroxylating the functional groups [10, 11]. However, the presence of sulphates not degrading under UV could have limited this damaging action, and allowed their survival under these conditions. These results are included in an article in review.

[1] J.P. Grotzinger *et al*., Science **343** (2014) 12427777.
[2] J.Guo *et al*., Astron. J. **155** (2018) 49.
[3] T. Milojevic *et al*., Commun. Earth Environ. **2** (2021) 39.
[4] D. Kölbl *et al.,* Front. Microbiol. **8** (2017) 1918.
[5] Y. Kawaguchi *et al*., Front. Microbiol. **11** (2020) 2050.
[6] T. Milojevic *et al.,* EGU **23** (2023) 16175.
[7] AR Santos *et al*., Geochim. Cosmochim. Acta **157** (2015) 56.
[8] MR Zierden and AM Valentine. Metallomics **8** (2016) 9.
[9] L.Z. Liu *et al.,* Res. Microbiol. **169** (2018) 590.
[10] G. Sarret *et al*., Geochim. Cosmochim. Acta **63** (1999) 3767.
[11] J. Cadet, J. and J.R. Wagner, J. R. Cold Spring Harbor Perspect. Biol. **5** (2013) a012559.